Inorganic Chemistry

pubs.acs.org/IC

Article

Pyrrolidinium-Based Cyanides: Unusual Architecture and Dielectric Switchability Triggered by Order–Disorder Process

Monika Trzebiatowska,* Mirosław Mączka, Anna Gagor, and Adam Sieradzki

Cite This: *Inorg. Chem.* 2020, 59, 8855–8863

Read Online

ACCESS | Metrics & More | Article Recommendations | Supporting Information

ABSTRACT: Two three-dimensional metal–organic compounds of the formula $Pyr_2KM(CN)_6$, where M = Co, Fe and Pyr = pyrrolidinium ($(CH_2)_4NH_2^+$), have been found to crystallize at room temperature in a monoclinic structure, space group $P2_1/c$. They are cyano-bridged compounds with an unprecedented type of architecture containing pyrrolidinium cations in the voids. The materials have been investigated by X-ray diffraction, dielectric, and spectroscopic methods as a function of temperature in order to determine their properties and the mechanism of the reversible phase transitions occurring at ca. 345–370 K. The phase transitions in both crystals are first order and are associated with a symmetry increase to a rhombohedral structure (space group $R\bar{3}m$) as well as a significant disorder of organic cations above T_c. On the basis of Raman scattering and IR spectroscopy it has been assumed that the phase transition in both crystals is triggered by thermally induced pseudorotation of the organic cation and large out-of-plane motions of its atoms followed by a "click-in" of the cyanide bridges. The materials have been proposed as possible switchable dielectrics due to their respective high differences in dielectric permittivities across the phase transition.

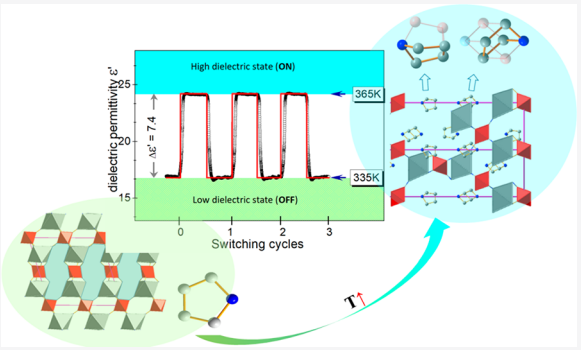

INTRODUCTION

The hybrid organic–inorganic perovskites based on diatomic and multiatomic bridges, which are built of $M^{II}O_6$ or $M^{II}N_6$ octahedra (M^{II} = Cd, Mg, Zn, Mn, Co, Fe, Cu, Ni) connected by short organic linkers (for instance, $HCOO^-$, N_3^-, CN^-, $N(CN)_2^-$, and HPO_2^-), have been extensively studied in recent years due to their magnetic, ferroelectric, multiferroic, ferroelastic, switchable dielectric, and barocaloric properties.[1−13] The characteristic feature of these materials is the presence of large voids occupied by organic ions. The properties of these compounds have been determined, among others, by the size, shape, and ability of the organic cation to form hydrogen bonds (HBs) with the anionic framework. For instance, the polar order and switchable dielectric properties appear due to ordering–disordering of these organic cations.[2,9,13−16]

Hybrids with CN^- ligands have been less studied in comparison to the formate analogues. Up to now, four $A_2KCo(CN)_6$ (A = methylammonium (MA), dimethylammonium (DMA), azetidinium (AZE), formamidinium (FM)) and eight $A_2KFe(CN)_6$ (A = MA, DMA, trimethylammonium (TrMA), tetramethylammonium (TMA), guanidinium (GA), acetamidinium (Ace), imidazolium (HIm), trimethylammonium oxide ($(CH_3)_3NOH$, TrMO)) cyanides have been synthesized.[15−23] The research on MA, TrMA, TMA, AZE, HIm, TrMO, and FM analogues has shown that these compounds exhibit single order–disorder phase transitions (PTs) accompanied by a distortion of the metal cyanide frameworks.[15−21] These transitions lead to steplike dielectric anomalies with a change in the real part of the dielectric permittivity ε' that is typically below 10.[15,19,21] Much larger changes, about 18 at 1 MHz and 30 at 2 MHz, were reported only for $(Him)_2KFe(CN)_6$ and $(MA)_2KCo(CN)_6$, respectively.[17,20] In contrast to this behavior, two-step order–disorder PTs were reported for $(DMA)_2KFe(CN)_6$, $(Ace)_2KFe(CN)_6$, and $(GA)_2KFe(CN)_6$.[18,22] The LT PTs in $(DMA)_2KFe(CN)_6$ and $(Ace)_2KFe(CN)_6$ and HT PT in $(GA)_2KFe(CN)_6$ lead to weak steplike anomalies of ε' (less than 10).[18,22] An increase in ε' has also been noticed at HT PT in $(DMA)_2KFe(CN)_6$, but the value of this change is not clear, since the PT occurs only a few degrees below the decomposition temperature.[18] It is worth adding that for $(MA)_2KCo(CN)_6$ the steplike anomaly strongly increases when the frequency changes from 1 kHz to 135 Hz, and this behavior has been attributed to a large contribution of the ac conductivity.[17] Furthermore, Fe analogues have often shown the presence of dielectric relaxation[17,18] but in the case of Co-

Received: February 28, 2020
Published: June 18, 2020

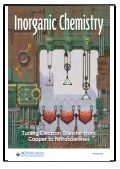

based compounds dielectric relaxation has only been reported for $(FA)_2KCo(CN)_6$.[21]

Herein, we report the synthesis and detailed studies of two Co and Fe cyanide frameworks (for simplicity referred to hereafter as **1Co** and **2Fe**) templated with pyrrolidinium (Pyr^+) cations. The Pyr^+ cations have not yet been employed in a synthesis of any perovskite-like materials. We will show that these compounds crystallize in an architecture different from that other cyanides and they exhibit switchable dielectric properties and unusually large frequency dependence of the steplike anomaly. We will discuss the origin of this behavior.

EXPERIMENTAL DETAILS

Synthesis. All reagents (analytical grade) used for the synthesis were commercially purchased from Sigma-Aldrich and used without further purification. In order to grow single crystals of **1Co and 2Fe** a mixture containing 2.6 mL of pyrrolidine (30 mmol) and 20 mL of water was neutralized with about 3 mL of hydrochloric acid. Then 5 mmol of $K_3M(CN)_6$ was dissolved in this solution on a hot plate at 50 °C with stirring. After 3 h the heating was switched off and the solutions were allowed to stand at room temperature. The rhombic crystals (dark orange for **2Fe** and pale yellow for **1Co**) were harvested after 1 week. A comparison of their powder XRD patterns with the calculated patterns based on the single-crystal data attest to the phase purity of powdered samples (Figure S1 in the Supporting Information).

X-ray Diffraction. The powder X-ray diffraction was measured on an X'Pert PRO powder diffractometer operating with Cu Kα radiation. The diffractograms were collected in the Bragg–Brentano geometry using fixed-divergence slits.

The single-crystal X-ray diffraction experiments were carried out with Mo Kα radiation using Xcalibur (Atlas). The absorption was corrected by Multiscan method in CrysAlis PRO 1.171.38.43 (Rigaku Oxford Diffraction, 2015). The empirical absorption correction using spherical harmonics, implemented in the SCALE3 ABSPACK scaling algorithm, was applied. The structures were solved by direct methods in SHELXT and refined with SHELXL2014/7.[23] The hydrogen atoms were placed in calculated positions and refined as riding atoms. Due to the complex disorder of protonated amines the hydrogen atoms were not introduced during the refinement of HT phases. The data have been assigned the following CCDC (Cambridge Crystallographic Data Centre) deposition numbers: 1969449–1969452.

Calorimetric and Dielectric Measurements. The heat capacity was measured using a Mettler Toledo DSC-1 calorimeter with a high resolution of 0.4 μW. Nitrogen was used as a purging gas, and the heating and cooling rate was 5 K/min. The excess heat capacity associated with the PT was evaluated by subtraction of the baseline, representing variation in the absence of the PTs, from the data.

The dielectric measurements were performed every 1 K using a Novocontrol Alpha impedance analyzer. The temperature was controlled by the Novo-Control Quattro system, by using a nitrogen gas cryostat. The temperature stability of the samples was better than 0.1 K. The dimensions of the single crystals with crystallographic orientations perpendicular to the (011) plane were 1.7 × 1.2 × 0.7 mm^3 for **2Fe** and 1.9 × 1.3 × 0.6 mm^3 for **1Co**, respectively. Silver paste was used to ensure a good electrical contact. The ac voltage with an amplitude of 1 V and frequency in the range 1 kHz to 1 MHz was applied across the sample. Each switching cycle was registered as time-dependent dielectric permittivity for 30 min at two constant temperatures. The temperature ramp between these temperatures was kept as 5 K/min.

IR and Raman Spectroscopy. The temperature-dependent IR spectra were measured in a heating mode on a KBr pellet in the range 4000–550 cm^{-1} using a standalone Nicolet iN10 microscope equipped with a liquid nitrogen cooled mercury–cadmium–telluride detector, permanently aligned 15× objective, and 0.7 numerical aperture with the working distance set at 16 mm. The Raman spectra were measured in a heating mode using a Renishaw InVia Raman spectrometer equipped with a confocal DM 2500 Leica optical microscope, a thermoelectrically cooled CCD as a detector, and an Ar^+ laser operating at 488 nm. Due to the bad quality of the signal from **2Fe** crystals, only the **1Co** sample was measured. The temperature of the samples during Raman and IR measurements was controlled applying a Linkam THMS 600 Heating/Freezing Stage. The spectral resolution in Raman and IR measurements was set at 2 cm^{-1}.

RESULTS AND DISCUSSION

DSC. The DSC measurements reveal one heat anomaly at 368 K (361 K) for **1Co** and at 354 K (346 K) for **2Fe** upon heating (cooling) (Figure 1 and Figure S2). The symmetrical

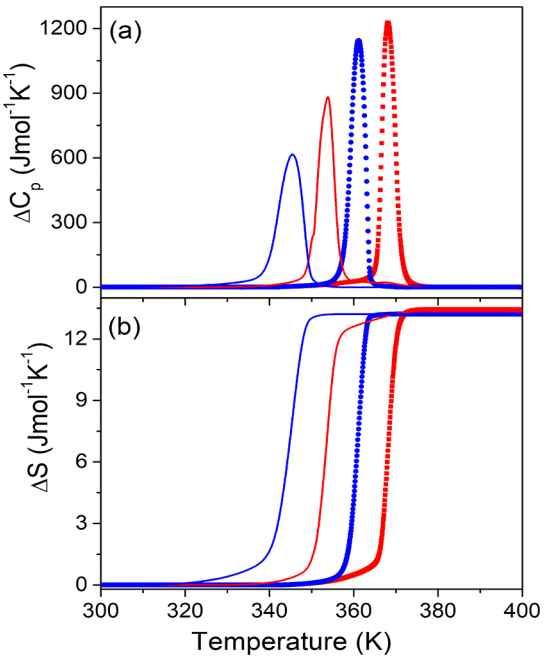

Figure 1. Temperature dependence of (a) C_p and (b) ΔS related to the PTs in **1Co** (circles and squares) and **2Fe** (solid lines) in heating (red) and cooling (blue) runs.

shape of these anomalies and significant thermal hysteresis point to first-order character of the PTs. The associated change in enthalpy ΔH and entropy ΔS are estimated for **1Co** to be ~4.7 kJ mol^{-1} and ~13.3 J mol^{-1} K^{-1}, respectively. Similar values, ~4.3 kJ mol^{-1} and ~13.2 J mol^{-1} K^{-1}, respectively, are found for **2Fe**. For an order–disorder transition $\Delta S = R \ln N$, where R is the gas constant and N is the ratio of the number of configurations in the disordered and ordered phases. The estimated N value associated with heat anomalies is about 4.9. A very large value of N indicates that the HT phases are strongly disordered. In the FM analogues the entropy values are on the order of 40 J mol^{-1} K^{-1}, while for an HIm-cyanide crystal it amounts to ca. 6.6 J mol^{-1} K^{-1}.[20,21]

Crystal Structures. The crystal structures of **1Co** and **2Fe** are isomorphic at RT as well as after the PT to the HT phase (Table 1). Both compounds crystallize in the monoclinic system with $P2_1/c$ symmetry; however, the architecture differs from those of other known cyanides. The asymmetric unit contains two M atoms located at the inversion center (C_i), one K, six cyanide C≡N ligands, and two ordered Pyr^+ cations. All atoms except M occupy general positions of C_1 symmetry. In the inorganic part of the structure each M(1) is surrounded by six K centers at a distance of ~5.9 Å similarly to other

https://dx.doi.org/10.1021/acs.inorgchem.0c00637
Inorg. Chem. 2020, 59, 8855–8863

Table 1. Experimental Details of Single-Crystal X-ray Diffraction Experiments

	1Co phase I	1Co phase II	2Fe phase I	2Fe phase II
		Crystal Data		
chem formula	$C_{14}H_{20}CoKN_8$	$C_{14}H_{20}CoKN_8$	$C_{14}H_{20}FeKN_8$	$C_{14}H_{20}FeKN_8$
M_r	398.41	398.41	395.33	395.33
cryst syst, space group	trigonal, $R\bar{3}m$:H	monoclinic, $P2_1/c$	trigonal, $R\bar{3}m$:H	monoclinic, $P2_1/c$
temp (K)	375	295	365	281
a, b, c (Å)	8.8604(4), 8.8604(4), 41.342(2)	14.3134(5), 8.9546(2), 15.0150(5)	8.8920(4), 8.8920(4), 41.596(2)	14.4144(5), 8.9694(2), 15.0356(5)
α, β, γ (deg)	90, 90, 120	90, 107.216(3), 90	90, 90, 120	90, 107.297(3), 90
V (Å^3)	2810.8(3)	1838.26(10)	2848.3(3)	1856.02(10)
Z	6	4	6	4
μ (mm^{-1})	1.15	1.17	1.03	1.05
cryst size (mm)	0.23 × 0.19 × 0.1	0.23 × 0.19 × 0.1	0.22 × 0.17 × 0.05	0.30 × 0.21 × 0.08
		Data Collection		
T_{min}, T_{max}	0.824, 1.000	0.927, 1.000	0.870, 1.000	0.950, 1.000
no. of measd, indep, and obsd ($I > 2\sigma(I)$) rflns	9641, 718, 612	19241, 3755, 2940	3725, 725, 517	27497, 3543, 2352
R_{int}	0.022	0.024	0.031	0.049
$(\sin\theta/\lambda)_{max}$ (Å^{-1})	0.609	0.625	0.610	0.625
		Refinement		
$R(F^2 > 2\sigma(F^2))$, $R_w(F^2)$, S	0.103, 0.336, 1.12	0.036, 0.098, 1.11	0.075, 0.231, 1.11	0.052, 0.135, 1.09
no. of rflns	718	3755	725	3543
no. of params	44	221	68	220
no. of restraints	8	12	6	12
H atom treatment	H atom params not defined	H atom params constrained	H atom params not defined	H atom params constrained
$\Delta\rho_{max}$ $\Delta\rho_{min}$ (e Å^{-3})	1.59, −0.91	0.66, −0.42	0.38, −1.11	0.56, −0.51

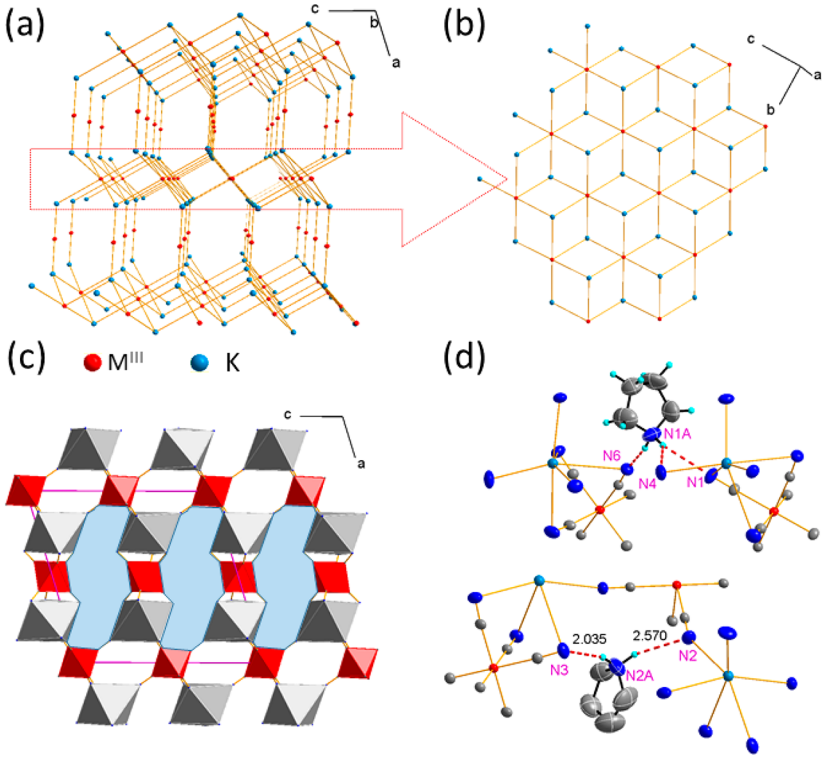

Figure 2. $Pyr_2KM(CN)_6$, LT phase II, $P2_1/c$. (a) The topology of MK cyanides. (b) A pseudotrigonal arrangement of M(1)−K layers. (c) Metal cyanide framework with an octahedral environment of metal ions. The channels in the structure are highlighted by blue shading. (d) In LT phases there are two inequivalent Pyr^+ cations, both interacting with the metal cyanide framework through the N−H···N HBs.

cyanides,[21] forming (011) layers with a pseudotrigonal atom arrangement. The layers are linked by nodes consisting of M(2)−$(CN)_6$, that possess only two K neighbors at a much reduced distance of 4.0 Å (Table S1). This yields a 3D arrangement with pronounced channels expanding in the b direction, which are populated with Pyr^+. This architecture resembles the pillar-layered structures,[24] though the pillars here are strictly inorganic. Figure 2a,b shows the topology of

https://dx.doi.org/10.1021/acs.inorgchem.0c00637
Inorg. Chem. 2020, 59, 8855−8863

1Co and **2Fe**; Figure 2c highlights the crystal voids. The cyanide ligands compose a distorted-octahedral environment around metal centers in both **1Co** and **2Fe** and M(2) links with two neighboring K centers via three cyanide bridges that strongly shapes the spheres of both KN_6 and $M(2)C_6$.

In the RT phase (I) the cations are ordered and anchored in the structure through N−H···N HBs to the cyanide nitrogen atoms. Figure 2d shows the close surrounding of symmetry-independent Pyr^+. In both **1Co** and **2Fe** each Pyr^+ forms one strong HB with the metal cyanide framework with a donor−acceptor (D-A) distance of 2.88(1) Å (the detailed values are given in Table 2). The remaining hydrogen atoms from NH_2 groups are involved in weaker interactions with D−A distances ranging from 3.07(1) to 3.35(1) Å. The respectively large atomic displacement parameters for ring carbons indicate a certain freedom of movement of the cations in this phase, possibly thermally activated.

Table 2. Selected HB Parameters

D−H···A	D−H (Å)	H···A (Å)	D···A (Å)	D−H···A (deg)
		Co Phase II		
N1A−H10A···N1	0.89	2.48	3.065(3)	123.7
N1A−H10B···N6[a]	0.89	2.00	2.875(3)	167.1
N2A−H13A···N3[a]	0.89	2.03	2.876(4)	159.3
N2A−H13B···N2[b]	0.89	2.58	3.351(4)	145.6
		Fe Phase II		
N1A−H10A···N1	0.89	2.50	3.076(5)	122.7
N1A−H10B···N6[a]	0.89	2.02	2.890(5)	166.5
N2A−H13A···N3[a]	0.89	2.04	2.888(6)	160.2
N2A−H13B···N2[b]	0.89	2.57	3.344(6)	145.8

[a]Symmetry code: $x, -y + 1/2, z - 1/2$. [b]Symmetry code: $-x, -y + 1, -z$.

The PT, recorded at T_c = 368/361 K in **1Co** and T_c = 354/346 K in **2Fe**, is accompanied by an increase of symmetry to rhombohedral, $R\bar{3}m$. The new unit cell is related to the LT cell by the [1 −1 0 1 1 0 −1/3 1/3 1/3] matrix. The Z value increases from 4 to 6 in phase I. Thus, despite the symmetry increase the asymmetric unit contains, similarly to phase II, the same number of metal atoms: two independent M ions, here at $-3m$ (D_{3d}) symmetry, and K at a $3m$ (C_{3v}) site. The presence of a 3-fold axis defines the environment of the metal centers. The number of symmetry-independent C≡N groups is reduced to two, each one being linked to one individual M center. The cyanide bridges that connect M(2) nodes with two neighboring K centers have much larger atomic displacement parameters in comparison to those of M(1).

The increasing temperature activates the thermal motions of Pyr^+. Similarly to LT phase, there are two different ammonium cations; however, in phase I they are both disordered. One Pyr^+ may adopt at least three various positions. As the nitrogen atom is located on a 3-fold axis these positions are related by the rotation of carbon ring atoms around the axis. Additionally, the ammonium nitrogen atom significantly leans out of the plane defined by the ring carbons. In **2Fe** the disorder is even larger; a satisfactory refinement is obtained with an almost spherical distribution of carbon and amine nitrogen atoms. Figure 3 presents the packing of phase I and the resolved disorder of both ammonium cations as well as the environment of Co(2) and K metals with the triple cyanide bridges.

The disorder related to the presence of the 3-fold axis is apparent in many crystals accommodating nicollite or hexagonal symmetries.[2,27,28] Usually, the disorder is dynamic and is thermally activated. Freezing of the cation motions along a decrease in temperature induces PTs. The LT phases of pyrrolidinium-based organic−inorganic hybrids often possess ferroelectric or even multiferroic properties.[27,28]

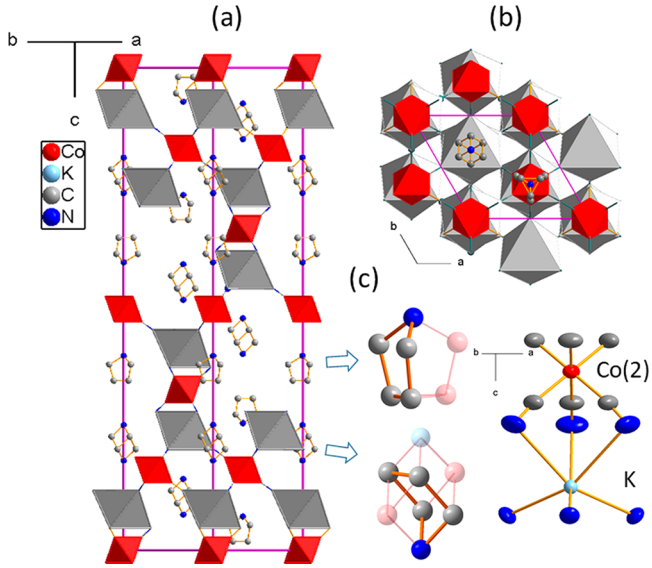

Figure 3. $Pyr_2KCo(CN)_6$, HT phase I. Views of the crystal structure along the (a) [110] and (b) [001] directions. (c) There are two distinct Pyr^+ cations in I; both are disordered via a 3-fold axis, and the 3-fold symmetry also determines the arrangement of cyanide ligands around metal centers.

Dielectric Studies. For both investigated compounds the steplike anomalies of the real part (ε') of the dielectric permittivity are observed around T_c in the heating and cooling modes, revealing a reversible PT (Figure 4). With the LT phase as a starting point, the ε' value increases from about 15−17 before the temperature reaches the PT point, corresponding to the low dielectric state. A further temperature increase results in sharp steplike dielectric anomalies to ∼23−25 at T_c, corresponding to a high dielectric state. Such a sharp dielectric anomaly around T_c is a typical characteristic for switchable dielectric materials. For **1Co** the dielectric permittivity ε' value in the high dielectric state is roughly 1.5 times of that in the low dielectric state. Moreover, for all frequencies this difference remains unchanged. In the case of **2Fe** above T_c a significant dispersion can be noticed, resulting in strong changes of ε' with decreasing probing frequency.

Generally, such behavior in the frameworks based on cyanide ligands is related to structural changes starting from the phase where organic cations are frozen to the orientationally disordered phase, which consequently leads to a significant change in the dielectric constant.[14,20−32] Thus, the difference in the observed frequency dispersions of **1Co** and **2Fe** indicates the disparate range of resonant frequencies attributed to the dynamic motion of the organic cation. Taking the above findings into consideration, we can conclude that for **2Fe** the interaction between the Pyr^+ and the framework is stronger in comparison to that in the **1Co** crystal, which is consistent with the crystallographic data. The PT temperatures match the DSC results well, which clearly indicates the reversible thermally triggered structural PTs. A small thermal hysteresis observed during the heating and cooling processes is comparable with those observed in the DSC results.

https://dx.doi.org/10.1021/acs.inorgchem.0c00637
Inorg. Chem. 2020, 59, 8855−8863

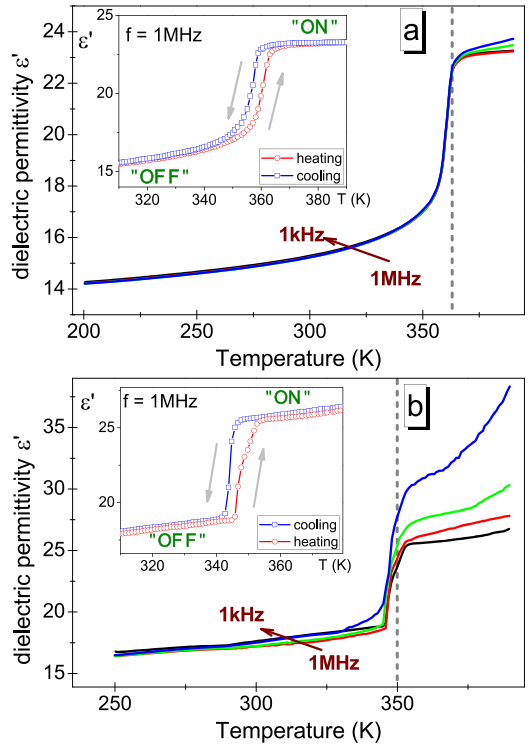

Figure 4. Temperature dependence of the real part of the dielectric permittivity (ε') measured for **1Co** (a) and **2Fe** (b) single crystals at selected frequencies during the heating cycle. The inset presents the heating (red) cycles and cooling (blue) cycles for f = 1 MHz.

The desired switchable behaviors of dielectric permittivities between the high and low dielectric states in the investigated compounds classify them as potential HT switchable materials (see Figure 5 and Figure S3). Close to discontinuous switching

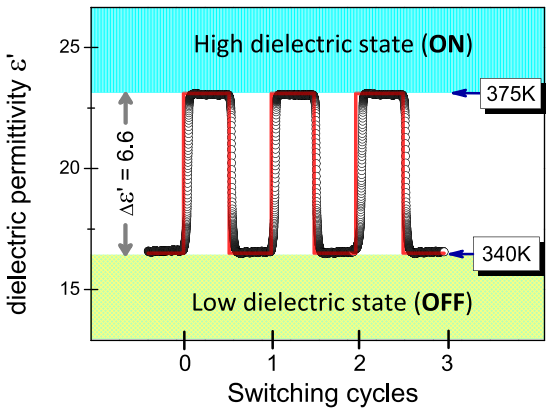

Figure 5. Reversible dielectric switching (ON and OFF) of ε' between HT and LT phases measured for **1Co** at a probing frequency of 1 MHz.

of the ε' value between the two stable dielectric states is related to rapid symmetry breaking during the structural PT, resulting from the order−disorder transition of Pyr^+ and the deformation of the framework. It can be noticed that both **1Co** and **2Fe** crystals exhibit a tendency to stable resistance to fatigue. As illustrated in Figure 5, ε' switching is stable and remains unchanged after at least three cycles. In each cycle, the low and high dielectric states represent "switch off" and "switch on", respectively. When the temperature goes through the PT point, ε' increases quickly from the low dielectric state to the high dielectric state, and when the temperature is lowered, the ε' value decreases reversibly from the high dielectric state to the low dielectric state. With the temperature repeatedly changing above or below the PT temperature, dielectric permittivity switching is observed. The repetition of ON/OFF cycles suggests the possible electronic application of the investigated compounds.

Raman Scattering and IR Studies. Table S2 shows the results of the factor group analysis for both **1Co** and **2Fe** samples, while the observed IR and Raman modes along with their assignment are given in Table S3. IR and Raman spectra in the full range are presented in Figures S4 and S5 for **1Co** as well as in Figure S6 for the **2Fe** analogue, respectively. The details of the IR and Raman spectra for **1Co** are presented in Figures 6 and 7, while details of IR spectra for **2Fe** are given in Figure S7. The assignment has been proposed on the basis of the literature data available for other similar compounds: cyanides and the compounds containing Pyr^+ as well as a related cyclopentane.[21,33−37] The thermal evolution of the bands, as described below, is based mainly on the changes of the **1Co** compound due to the fact that both cyanides are isostructural and behave in a similar fashion upon temperature change. Figure 8 and Figures S8 and S9 present the temperature-dependent evolution of the position and/or the bandwidth (fwhm) of several selected modes of **1Co** and **2Fe** crystals, respectively, in order to get insight into the mechanism of the transitions.

There are two types of HBs in **2Fe** and **1Co** samples, i.e. medium and strong,[38] one with a donor−acceptor distance of ca. 3.07−3.35 Å being located at roughly 3200 cm^{-1}, while the other is present at about 2800 cm^{-1} with a length equal to *ca.* 2.88 Å. The Raman and IR spectra of the studied compounds show many characteristic changes as a function of temperature.

First, narrowing of many IR and Raman bands on a decrease in temperature is observed for both compounds, with a clear discontinuous jump at the PT temperature (Figures 6−8 and Figures S4−S7 and S9). This is especially characteristic of the bands assigned to the NH_2 vibrations, such as $\nu(NH_2)$ stretching modes present in the region 3260−2730 cm^{-1} (Figure 8a and Figure S9a for **1Co** and **2Fe**, respectively), $\delta(NH_2)$ bending modes present at ca. 1630−1590 cm^{-1} (Figure 6 and Figure S7 for **1Co** and **2Fe**, respectively), $\omega(NH_2)$ and $\tau(NH_2)$ bending modes at 1400−1230 cm^{-1} (Figures 6, 7, and 8d,f for **1Co** and Figures S7 and S9d for **2Fe**), and $\rho(NH_2)$ bending modes at 880−820 cm^{-1} (Figures 6, 7, and 8f for **1Co** and Figures S7 and S9d for **2Fe**). This behavior is consistent with an ordering of the Pyr^+ cations. Thus, temperature-dependent Raman and IR spectra confirm the order−disorder mechanism of the PTs, similarly to those found in DMA metal formates or the FA-based perovskites mentioned above.[21,39,40] It worth adding that the change in fwhm values is not as distinct as that observed before for other similar compounds. For instance, the Raman mode of **1Co** at ca. 880 cm^{-1} presents a 1.3 increase in fwhm on going from the LT to HT phase against a 4-fold increase in $FA_2KCo(CN)_6$.[21] Interestingly, many bands of the studied compounds remain broad below T_c and exhibit further significant narrowing on cooling (see for instance the temperature dependence of fwhm for the ring + $\rho(CH_2)$ and $\rho(NH_2)$ Raman-active modes in Figure 8e,f), which indicates that the Pyr^+ cations possess a large degree of motional freedom even much below T_c.

https://dx.doi.org/10.1021/acs.inorgchem.0c00637
Inorg. Chem. 2020, 59, 8855−8863

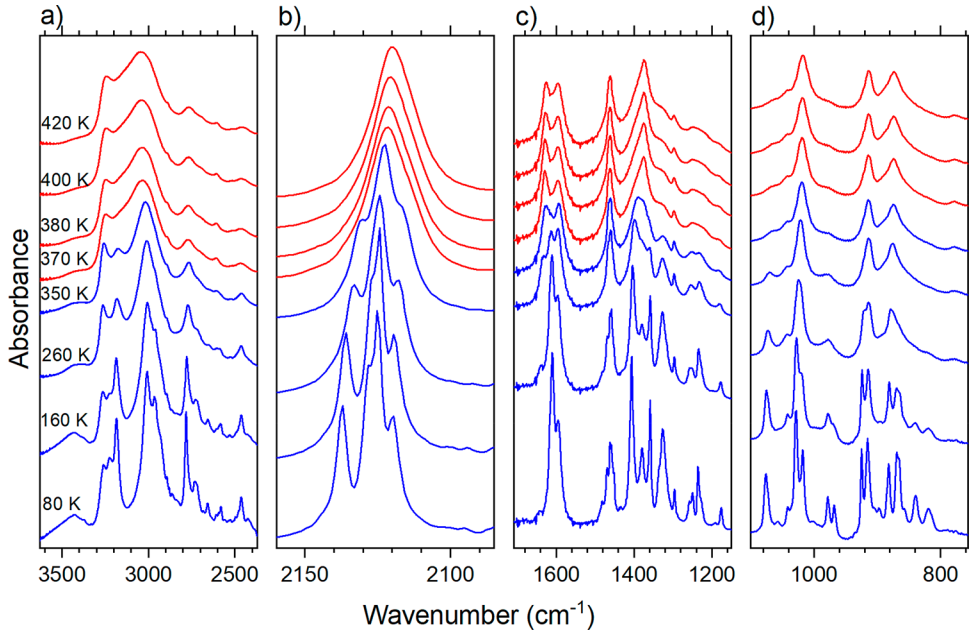

Figure 6. Details of the temperature-dependent IR spectra of **1Co**.

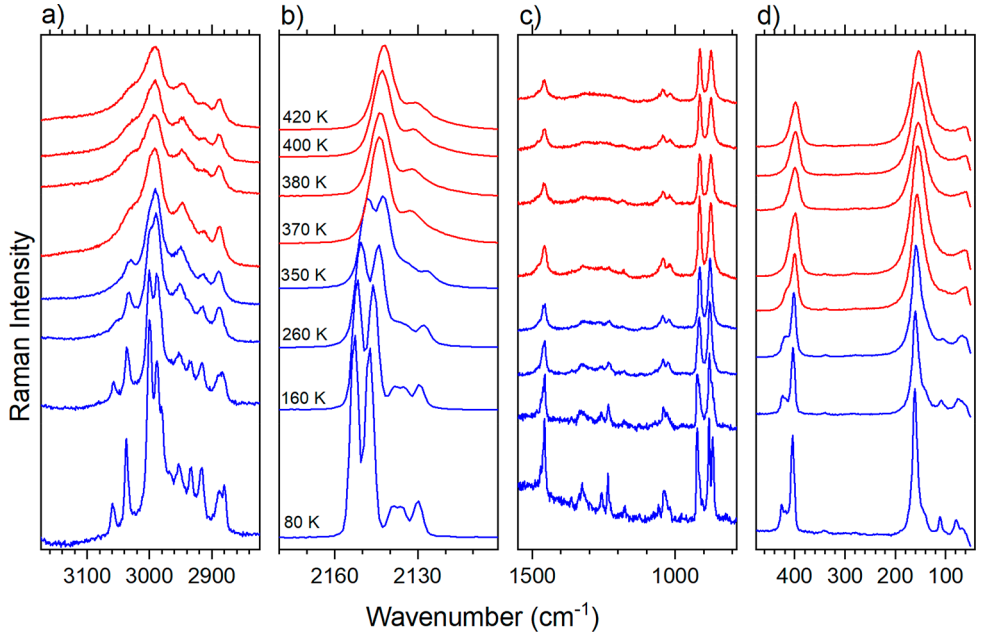

Figure 7. Details of the temperature-dependent Raman spectra of **1Co**.

Second, many bands split into a few components with a decrease in temperature, which is consistent with the lowering of symmetry. Furthermore, many bands exhibit abrupt shifts at T_c. For some modes related to HBs these shifts are as distinct, as in the case of perovskite crystals studied by us before: e.g., formamidinium Mn-formate, $(FA)_2KM(CN)_6$, DMA-based formates, and azides.[21,39,40,42] For example, the NH_2 stretching mode, observed near 3040 cm^{-1} in the HT phase, shifts to lower wavenumbers in the LT phase (by ca. 20 cm^{-1}, Figure 8a and Figure S9a for **1Co** and **2Fe**, respectively), while the $\omega(NH_2)$ mode exhibits an upshift of about 33 cm^{-1} (Figure 8d). The maxima of the remaining HB-related modes experience lesser shifts, though much stronger than those reported for other systems: e.g., FA-based cyanides. This implies that the phase transition leads to a significant rearrangement of the HB network. It is important to note that, in spite of rapid movements of the organic cations at elevated temperatures and the rearrangement of HBs, there is still a division of their strength into medium and strong, as the two groups of the bands originating from HBs are preserved. In contrast to the NH_2 modes, the ring vibrations show weaker wavenumber shifts at T_c (see Figure 8b,e and Figure S9c for **1Co** and **2Fe**, respectively). These shifts go along with the shortening of the C−H bonds within Pyr^+ cations in the LT phase. Thus, all the facts suggest that the ordering of Pyr^+ cations below T_c strongly influences their conformation. This behavior has been attributed to a respectively high flexibility of the ring.[36]

https://dx.doi.org/10.1021/acs.inorgchem.0c00637
Inorg. Chem. 2020, 59, 8855−8863

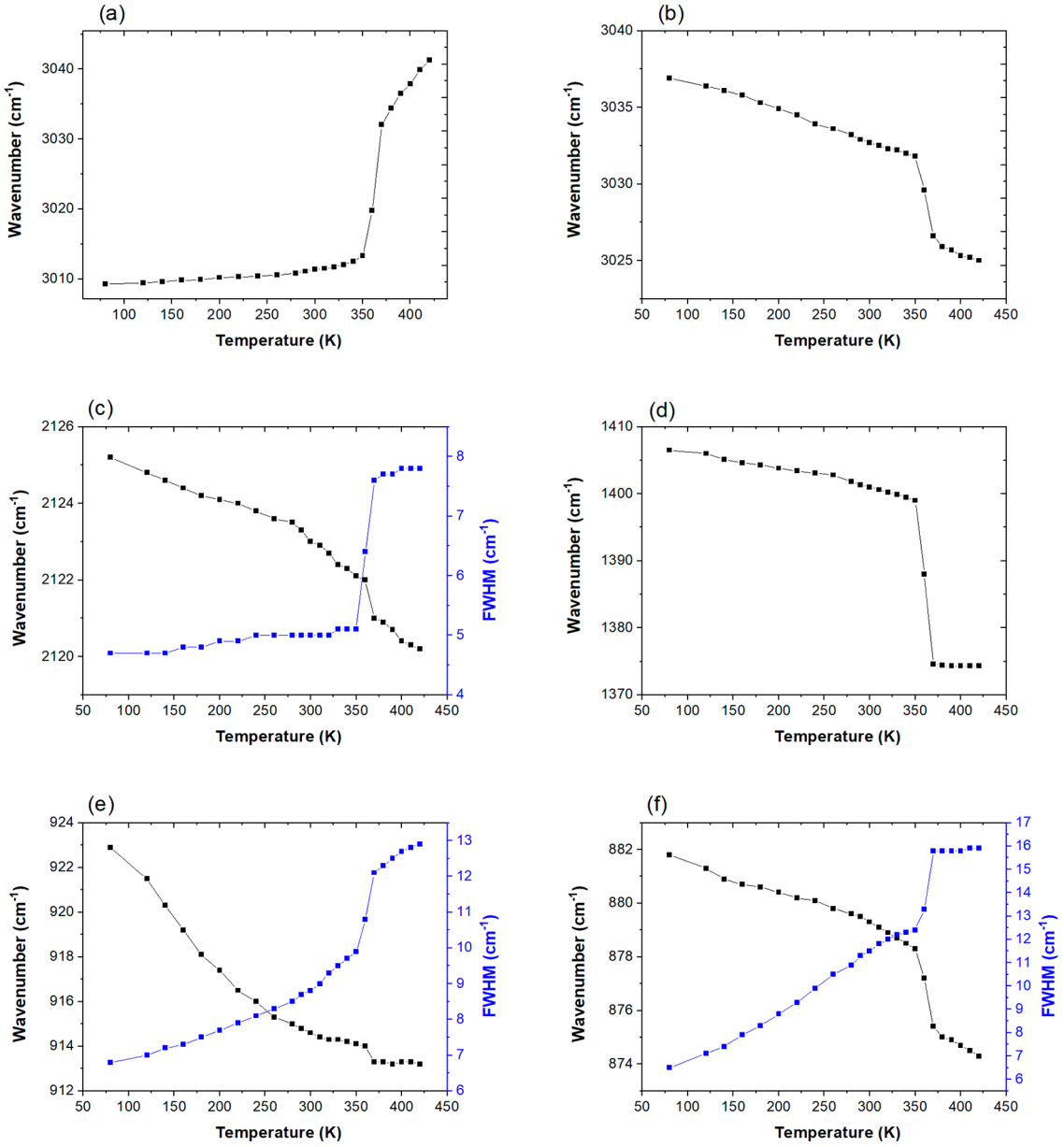

Figure 8. Plots of the wavenumber and fwhm vs T of the selected modes (a) $\nu_s(NH_2)$ (IR), (b) $\nu_{as}(CH_2)$ (Raman), (c) $\nu(CN^-)$ (IR), (d) $\omega(NH_2)$ (IR), (e) ring + $\rho(CH_2)$ (Raman), and (f) $\rho(NH_2)$ (Raman) in **1Co**.

Third, the characteristic feature is the continuous wavenumber shift of the bands well ahead of their phase transition point. This refers to both the pyrrolidinium cations and cyanide ions, unlike the case of FA analogues or azide systems.[40,41] (see Figure 8b,e and Figure S9c for **1Co** and **2Fe**, respectively, for C−H vibrations). This difference indicates that the change in temperature has a much stronger effect on pyrrolidinium−framework interactions in comparison to cyanide- and azide-based perovskite-like materials. Such behavior can be most likely be attributed to the conformation of the Pyr^+ cation that allows large out-of-plane motions of atoms. As a result, slowing down of thermally activated motions upon cooling significantly affects HB strength and thus chemical bonds and angles in the organic cation and metal cyanide frameworks.

Fourth, the PTs in both crystals lead to pronounced vibrational changes in the metal cyanide frameworks (see Figures 6, 7, and 8c and Figure S8a for **1Co**, and Figures S6 and S9b for **2Fe**, respectively). For instance, the stretching mode observed at ca. 2125/2150 cm^{-1} in the IR/Raman spectrum of **1Co** shifts by roughly 6/10 cm^{-1} in the whole temperature range with a noticeable wavenumber upshift (∼1 cm^{-1} and fwhm decrease at the PT point during cooling (Figure 8c and Figure S8a for **1Co** and Figure S9b for **2Fe**). The upshift informs us about the shortening of C≡N bonds, since the voids need to adjust to the ordering of the organic cations. A large shift in the whole temperature range, significantly larger in comparison to the other cyanide or azide analogues,[21,41,42] indicates a greater softness of the studied compounds. The fwhm of the stretching mode is much smaller in the HT phase (about 7.7 cm^{-1}, Figure 8c) than fwhm values of Pyr^+ modes (13−16 cm^{-1}, Figure 8e,f). This behavior is consistent with the fact that the cyanide linkers are ordered. Interestingly, the change in fwhm at T_c is quite large, about 2.5 cm^{-1}. This behavior indicates large thermal

https://dx.doi.org/10.1021/acs.inorgchem.0c00637
Inorg. Chem. 2020, 59, 8855−8863

movements of the CN^- group atoms in the HT phase and freezing of these movements in the LT phase.

CONCLUSIONS

Two metal−organic compounds of the formula $[Pyr_2KM(CN)_6]$, where M = Co, Fe, have been found to crystallize in an unusual architecture, with channels expanding in the *b* direction filled with Pyr^+ cations. They have been investigated by X-ray diffraction, dielectric, and spectroscopic methods in order to determine the mechanism of the PTs occurring within the ca. 345−370 K range. According to the obtained results they are first order and both crystals adopt isostructural architectures regarding LT and HT phases. To our knowledge this is an unprecedented representation of pyrrolidinium-templated compounds containing cyanides, related to the known cyano-bridged perovskite compounds and other metal−organic perovskite analogues.

The desired switchable behaviors of dielectric permittivities between the high and low dielectric states in the investigated compounds classify them as potential HT switchable materials. What is more important, the materials seem to be resistant to fatigue, and this indicates their possible electronic application.

Vibrational spectroscopy has been a very useful tool in the investigation of the mechanisms of PTs in these systems (though rarely used so far), as the most intense stretching band of the cyanides serves a perfect probe due to its isolation from the other bands as well as to the fact that both IR and Raman spectroscopy are sensitive to slight changes in bond lengths imposed by a crystal distortion. It has been observed that the movements of HBs are active well below the PT point, which indicates their dynamic nature even at LT. The Pyr^+ cations and specifically the HBs undergo drastic modifications at T_c and significant changes on a further temperature decrease below T_c. The thermal evolution of bands assigned to the cyanide ions is more pronounced than in the case of other cyanide-based perovskites. This behavior can be attributed to a softer nature of the studied compounds and a presence of strong HBs, which binds the Pyr^+ cations and one of the cyanide linkers quite tightly. Therefore, we assume that the PT in both crystals is triggered by thermally induced pseudorotation of the organic cation and large out-of-plane motions of its atoms followed by a "click-in" of the cyanide bridges.

ASSOCIATED CONTENT

Supporting Information

The Supporting Information is available free of charge at https://pubs.acs.org/doi/10.1021/acs.inorgchem.0c00637.

Crystallographic data, Raman and IR wavenumbers, XRD patterns, DSC traces, dielectric data, and IR and Raman spectra (PDF)

Accession Codes

CCDC 1969449−1969452 contain the supplementary crystallographic data for this paper. These data can be obtained free of charge via www.ccdc.cam.ac.uk/data_request/cif, or by emailing data_request@ccdc.cam.ac.uk, or by contacting The Cambridge Crystallographic Data Centre, 12 Union Road, Cambridge CB2 1EZ, UK; fax: +44 1223 336033.

AUTHOR INFORMATION

Corresponding Author

Monika Trzebiatowska − *Institute of Low Temperature and Structure Research, Polish Academy of Sciences, 50-950 Wrocław 2, Poland;* orcid.org/0000-0001-7975-5665; Email: mtrzeb@wp.pl

Authors

Mirosław Mączka − *Institute of Low Temperature and Structure Research, Polish Academy of Sciences, 50-950 Wrocław 2, Poland;* orcid.org/0000-0003-2978-1093

Anna Gagor − *Institute of Low Temperature and Structure Research, Polish Academy of Sciences, 50-950 Wrocław 2, Poland*

Adam Sieradzki − *Faculty of Fundamental Problems of Technology, Wrocław University of Science and Technology, 50-370 Wrocław, Poland;* orcid.org/0000-0003-4136-5754

Complete contact information is available at: https://pubs.acs.org/10.1021/acs.inorgchem.0c00637

Notes

The authors declare no competing financial interest.

ACKNOWLEDGMENTS

This research was supported by the National Science Center (Narodowe Centrum Nauki) in Poland under project No. 2017/25/B/ST5/00160.

REFERENCES

(1) Wang, Z.-M.; Zhang, B.; Otsuka, T.; Inoue, K.; Kobayashi, H.; Kurmoo, M. Anionic NaCl-type frameworks of $[Mn^{II}(HCOO)_3^-]$, templated by alkylammonium, exhibit weak ferromagnetism. *Dalton Trans.* **2004**, 2209−2216.

(2) Mączka, M.; Gągor, A.; Ptak, M.; Paraguassu, W.; da Silva, T. A.; Sieradzki, A.; Pikul, A. Phase Transitions and Coexistence of Magnetic and Electric Orders in the Methylhydrazinium Metal Formate Frameworks. *Chem. Mater.* **2017**, *29*, 2264−2275.

(3) Jain, P.; Dalal, N. S.; Toby, B. H.; Kroto, W.; Cheetham, A. K. J. Multiferroic Behavior Associated with an Order-Disorder Hydrogen Bonding Transition in Metal-Organic Frameworks (MOFs) with the Perovskite ABX_3 Architecture. *J. Am. Chem. Soc.* **2008**, *130*, 10450−10451.

(4) Chen, S.; Shang, R.; Hu, K.-L.; Wang, Z.-M.; Gao, S. $[NH_2NH_3][M(HCOO)_3]$ (M = Mn^{2+}, Zn^{2+}, Co^{2+} and Mg^{2+}): structural phase transitions, prominent dielectric anomalies and negative thermal expansion, and magnetic ordering. *Inorg. Chem. Front.* **2014**, *1*, 83−98.

(5) Mączka, M.; Pasińska, K.; Ptak, M.; Paraguassu, W.; Almeida da Silva, T.; Sieradzki, A.; Pikul, A. Effect of solvent, temperature and pressure on the stability of chiral and perovskite metal formate frameworks of $[NH_2NH_3][M(HCOO)_3]$ (M = Mn, Fe, Zn). *Phys. Chem. Chem. Phys.* **2016**, *18*, 31653−31663.

(6) (a) Wu, Y.; Shaker, S. M.; Brivio, F.; Murugavel, R.; Bristowe, P. D.; Cheetham, A. K. $[Am]Mn(H_2POO)_3$: A New Family of Hybrid Perovskites Based on the Hypophosphite Ligand. *J. Am. Chem. Soc.* **2017**, *139*, 16999−17002. (b) Wu, Y.; Binford, T.; Hill, J. A.; Shaker, S.; Wang, J.; Cheetham, A. K. Hypophosphite hybrid perovskites: a platform for unconventional tilts and shifts. *Chem. Commun.* **2018**, *54*, 3751−3754.

(7) Xu, W.-J.; Li, P.-F.; Tang, Y.-Y.; Zhang, W.-X.; Xiong, R.-G.; Chen, X.-M. A Molecular Perovskite with Switchable Coordination Bonds for High-Temperature Multiaxial Ferroelectrics. *J. Am. Chem. Soc.* **2017**, *139*, 6369−6375.

(8) Zhao, X.-H.; Huang, X.-C.; Zhang, S.-L.; Shao, D.; Wei, H.-Y.; Wang, X.-Y. Cation-Dependent Magnetic Ordering and Room-Temperature Bistability in Azido-Bridged Perovskite-Type Compounds. *J. Am. Chem. Soc.* **2013**, *135*, 16006−16009.

(9) Du, Z.-Y.; Xu, T.-T.; Huang, B.; Su, Y.-J.; Xue, W.; He, C.-T.; Zhang, W.-X.; Chen, X.-M. Switchable Guest Molecular Dynamics in a Perovskite-Like Coordination Polymer toward Sensitive Thermor-

esponsive Dielectric Materials. *Angew. Chem., Int. Ed.* **2015**, *54*, 914−918.
(10) Duncan, H. D.; Beake, E. O. R.; Playford, H. Y.; Dove, M. T.; Phillips, A. E. Local structure of a switchable dielectric Prussian blue analogue. *CrystEngComm* **2017**, *19*, 7316−7321.
(11) Bermúdez-Garcia, J. M.; Sánchez-Andújar, M.; Castro-García, S.; López-Beceiro, J.; Artiaga, R.; Señarís-Rodríguez, M. A. Giant barocaloric effect in the ferroic organic-Inorg. hybrid [TPrA][Mn(dca)$_3$] perovskite under easily accessible pressures. *Nat. Commun.* **2017**, *8*, 15715.
(12) Mączka, M.; Ptak, M.; Gągor, A.; Sieradzki, A.; Peksa, P.; Usevicius, G.; Simenas, M.; Furtado Leite, F.; Paraguassu, W. Temperature- and pressure-dependent studies of a highly flexible and compressible perovskite-like cadmium dicyanamide framework templated with protonated tetrapropylamine. *J. Mater. Chem. C* **2019**, *7*, 2408−2420.
(13) Zhao, M. M.; Zhou, L.; Shi, P.-P.; Zheng, X.; Chen, X.-G.; Gao, J.-X.; He, L.; Ye, Q.; Liu, C.-M.; Fu, D.-W. 3D Organic-Inorg. Perovskite Ferroelastic Mater. with Two Ferroelastic Phases: [Et$_3$P(CH$_2$)$_2$F][Mn(dca)$_3$] and [Et$_3$P(CH$_2$)$_2$Cl][Mn(dca)$_3$]. *Chem. - Eur. J.* **2019**, *25*, 6447−6454.
(14) Zhang, W.; Ye, H. Y.; Graf, R.; Spiess, H. W.; Yao, Y. F.; Zhu, R. Q.; Xiong, R. G. Tunable and Switchable Dielectric Constant in an Amphidynamic Crystal. *J. Am. Chem. Soc.* **2013**, *135*, 5230−5233.
(15) Xu, W.-J.; Chen, S.-L.; Hu, Z.-T.; Lin, R.-B.; Su, Y.-J.; Zhang, W.-X.; Chen, X.-M. The cation-dependent structural phase transition and dielectric response in a family of cyano-bridged perovskite-like coordination polymers. *Dalton Trans.* **2016**, *45*, 4224−4229.
(16) Shi, C.; Han, X. B.; Zhang, W. Structural phase transition-associated dielectric transition and ferroelectricity in coordination compounds. *Coord. Chem. Rev.* **2019**, *378*, 561−576.
(17) Rok, M.; Prytys, J. K.; Kinzhybalo, V.; Bator, G. Flexible crystals of perovskite-like coordination polymers with a tunable and switchable organic guest: (CH$_3$NH$_3$)$_2$[KFe(CN)$_6$] and (CH$_3$NH$_3$)$_2$[KCo(CN)$_6$]. *Dalton Trans.* **2017**, *46*, 2322−2331.
(18) Rok, M.; Bator, G.; Medycki, W.; Zamponi, M.; Balciunas, S.; Simenas, M.; Banys, J. Reorientational dynamics of organic cations in perovskite-like coordination polymers. *Dalton Trans.* **2018**, *47*, 17329−17341.
(19) Qian, K.; Zhao, F.; Yan, Z.; Pang, J.; Chen, X.; Yang, C. A perovskite-type cage compound as a temperature-triggered dielectric switchable material. *CrystEngComm* **2016**, *18*, 7671−7674.
(20) Zhang, W.; Cai, Y.; Xiong, R. G.; Yoshikawa, H.; Awaga, K. Exceptional Dielectric Phase Transitions in a Perovskite-Type Cage Compound. *Angew. Chem., Int. Ed.* **2010**, *49*, 6608−6610.
(21) Trzebiatowska, M.; Gągor, A.; Macalik, L.; Peksa, P.; Sieradzki, A. Phase transition in the extreme: a cubic-to-triclinic symmetry change in dielectrically switchable cyanide perovskites. *Dalton Trans.* **2019**, *48*, 15830−15840.
(22) Xu, W.-J.; Xie, K.-P.; Xiao, Z.-F.; Zhang, W.-X.; Chen, X.-M. Controlling Two-Step Phase Transitions and Dielectric Responses by A-Site Cations in Two Perovskite-like Coordination Polymers. *Cryst. Growth Des.* **2016**, *16*, 7212−7217.
(23) (a) Sheldrick, G. M. A short history of SHELX. *Acta Crystallogr., Sect. A: Found. Crystallogr.* **2008**, *A64*, 112−122. (b) Sheldrick, G. M. Crystal structure refinement with SHELXL. *Acta Crystallogr., Sect. C: Struct. Chem.* **2015**, *C71*, 3−8.
(24) ZareKarizi, F.; Joharian, M.; Morsali, A. *J. Mater. Chem. A* **2018**, *6*, 19288−19329.
(25) Mączka, M.; Gągor, A.; Marinho Costa, N. L.; Paraguassu, W.; Sieradzki, A.; Pikul, A. Temperature- and pressure-induced phase transitions in the niccolite-type formate framework of [H$_3$N(CH$_3$)$_4$NH$_3$][Mn$_2$(HCOO)$_6$]. *J. Mater. Chem. C* **2016**, *4*, 3185−3194.
(26) Mączka, M.; Ciupa, A.; Gągor, A.; Sieradzki, A.; Pikul, A.; Ptak, M. Structural, magnetic and dielectric properties of two novel mixed-valence iron(ii)-iron(iii) metal formate frameworks. *J. Mater. Chem. C* **2016**, *4*, 1186−1193.
(27) Ksiądzyna, M.; Gągor, A.; Piecha-Bisiorek; Ciżman, A.; Medycki, w.; Jakubas, R. Exploring a hybrid ferroelectric with a 1-D perovskite-like structure: bis(pyrrolidinium) pentachloroantimonate-(iii). *J. Mater. Chem. C* **2019**, *7*, 10360−10370.
(28) Wojciechowska, M.; Gagor, A.; Piecha-Bisiorek, A.; Jakubas, R.; Ciżman, A.; Zaremba, J.; Nyk, M.; Medycki, W.; Bil, A. Ferroelectricity and Ferroelasticity in Organic Inorg. Hybrid (Pyrrolidinium)$_3$[Sb$_2$Cl$_9$]. *Chem. Mater.* **2018**, *30*, 4597−4608.
(29) Zhang, X.; Shao, X.-D.; Li, S.-C.; Cai, Y.; Yao, Y.-F.; Xiong, R.-G.; Zhang, W. Dynamics of a caged imidazolium cation-toward understanding the order-disorder phase transition and the switchable dielectric constant. *Chem. Commun.* **2015**, *51*, 4568−4571.
(30) Rok, M.; Moskwa, M.; Działowa, M.; Bieńko, A.; Rajnák, C.; Boča, R.; Bator, G. Multifunctional Mater. based on the double-perovskite organic-Inorg. hybrid (CH$_3$NH$_3$)$_2$[KCr(CN)$_6$] showing switchable dielectric, magnetic, and semiconducting behavior. *Dalton Trans.* **2019**, *48*, 16650−16660.
(31) Rok, M.; Bator, G.; Zarychta, B.; Dziuk, B.; Skałecki, D. K.; Medycki, W.; Zamponi, M. Screening Ferroelastic Transitions in Switchable Cyano-Bridged Perovskites: [CH$_3$C(NH$_2$)$_2$]$_2$[KM(CN)$_6$], M = Cr^{3+}, Fe^{3+}, Co^{3+}. Crystal Structure Characterization, Dielectric Properties, 1H NMR, and Quasielastic Neutron Scattering Studies. *Cryst. Growth Des.* **2019**, *19* (8), 4526−4537.
(32) Shi, C.; Yu, C.-H.; Zhang, W. Predicting and Screening Dielectric Transitions in a Series of Hybrid Organic-Inorg. Double Perovskites via an Extended Tolerance Factor Approach. *Angew. Chem., Int. Ed.* **2016**, *55*, 5798−5802.
(33) McCullough, R.; Jones, L.; Crosby, G. An analysis of the vibrational spectrum of the tetracyanonickelate(II) ion in a crystal lattice. *Spectrochim. Acta, Part A* **1960**, *16*, 929.
(34) Karaagaç, D.; Kürkçüoglu, G. S. Syntheses, spectroscopic and thermal analyses of cyanide bridged heteronuclear polymeric complexes: [M(L)$_2$Ni(CN)$_4$]$_n$ (LN-methylethylenediamine or N-ethylethylenediamine; MNi(II), Cu(II), Zn(II) or Cd(II)). *J. Mol. Struct.* **2016**, *1105*, 263−272.
(35) Evans, J. C.; Wahr, J. C. Thermodynamic and Spectroscopic Study of Pyrrolidine. II. Vibrational Spectra and Configuration. *J. Chem. Phys.* **1959**, *31*, 655−662.
(36) Carballeira, L.; Pérez-Juste, I. Ab initio study of the pseudorotation and conformational stability of pyrrolidine. *J. Chem. Soc., Perkin Trans. 2* **1998**, *2*, 1339−1345.
(37) Ocola, E. J.; Bauman, L. E.; Laane, J. Vibrational Spectra and Structure of Cyclopentane and its Isotopomers. *J. Phys. Chem. A* **2011**, *115*, 6531−6542.
(38) Steiner, T. The hydrogen bond in the solid state. *Angew. Chem., Int. Ed.* **2002**, *41*, 48−76.
(39) Maczka, M.; Ciupa, A.; Gagor, A.; Sieradzki, A.; Pikul, A.; Macalik, B.; Drozd, M. Perovskite Metal Formate Framework of [NH$_2$-CH$^+$-NH$_2$]Mn(HCOO)$_3$]: Phase Transition, Magnetic, Dielectric, Phonon Properties. *Inorg. Chem.* **2014**, *53*, 5260−5268.
(40) Mączka, M.; Pietraszko, A.; Macalik, L.; Sieradzki, A.; Trzmiel, J.; Pikul, A. Synthesis and order-disorder transition in a novel metal formate framework of [(CH$_3$)$_2$NH$_2$]Na$_{0.5}$Fe$_{0.5}$(HCOO)$_3$]. *Dalton Trans.* **2014**, *43*, 17075−17084.
(41) Trzebiatowska, M.; Ptak, M. The mechanism of phase transitions in azide perovskites probed by vibrational spectroscopy. *Spectrochim. Acta, Part A* **2019**, *214*, 184−191.
(42) Trzebiatowska, M.; Mączka, M.; Ptak, M.; Giriunas, L.; Balciunas, S.; Simenas, M.; Klose, D.; Banys, J. Spectroscopic Study of Structural Phase Transition and Dynamic Effects in a [(CH$_3$)$_2$NH$_2$]-[Cd(N$_3$)$_3$] Hybrid Perovskite Framework. *J. Phys. Chem. C* **2019**, *123* (18), 11840−11849.

https://dx.doi.org/10.1021/acs.inorgchem.0c00637
Inorg. Chem. 2020, 59, 8855−8863